Chaos
An Interdisciplinary Journal of Nonlinear Science

RESEARCH ARTICLE | SEPTEMBER 06 2024

Riddled basins of chaotic synchronization and unstable dimension variability in coupled Lorenz-like systems FREE

Special Collection: From Sand to Shrimps: In Honor of Professor Jason A. C. Gallas

Bruno M. Czajkowski ; Ricardo L. Viana

Check for updates

Chaos 34, 093113 (2024)
https://doi.org/10.1063/5.0219961

View Online
Export Citation

15 September 2024 03:59:26

AIP Publishing

Chaos
Special Topic:
Anomalous Diffusion and Fluctuations in Complex Systems and Networks
Submit Today
AIP Publishing

Riddled basins of chaotic synchronization and unstable dimension variability in coupled Lorenz-like systems

Cite as: Chaos 34, 093113 (2024); doi: 10.1063/5.0219961
Submitted: 21 May 2024 · Accepted: 19 August 2024 ·
Published Online: 6 September 2024

View Online Export Citation CrossMark

Bruno M. Czajkowski[1,a)] and Ricardo L. Viana[1,2]

AFFILIATIONS

[1]Departamento de Física, Universidade Federal do Paraná, 81531-990 Curitiba, Paraná, Brazil
[2]Universidade Federal do Paraná, Centro Interdisciplinar de Ciência, Tecnologia e Inovação, Núcleo de Modelagem e Computação Científica, Curitiba-PR, Brazil

Note: This paper is part of the Focus Issue, From Sand to Shrimps: In Honor of Professor Jason A. C. Gallas.
[a)]**Author to whom correspondence should be addressed:** bruno.czajkowski@ufpr.br

ABSTRACT

Unstable dimension variability is an extreme form of non-hyperbolic behavior that causes a severe shadowing breakdown of chaotic trajectories. This phenomenon can occur in coupled chaotic systems possessing symmetries, leading to an invariant attractor with riddled basins of attraction. We consider the coupling of two Lorenz-like systems, which exhibits chaotic synchronized and anti-synchronized states, with their respective basins of attraction. We demonstrate that these basins are riddled, in the sense that they verify both the mathematical conditions for their existence, as well as the characteristic scaling laws indicating power-law dependence of parameters. Our simulations have shown that a biased random-walk model for the log-distances to the synchronized manifold can accurately predict the scaling exponents near blowout bifurcations in this high-dimensional coupled system. The behavior of the finite-time Lyapunov exponents in directions transversal to the invariant subspace has been used as numerical evidence of unstable dimension variability.

Published under an exclusive license by AIP Publishing. https://doi.org/10.1063/5.0219961

15 September 2024 03:59:26

Dynamical systems of physical and biological interest often display multistable behavior, with a complicated structure of their basins of attractions. For example, if the boundary between two basins is a fractal set, a given improvement in the accuracy with which an initial condition is determined does not necessarily reflect in a corresponding reduction in the fraction of uncertain initial conditions, a phenomenon called final-state uncertainty. Riddled basins are extreme forms of fractal behavior, leading to practically no decrease of this uncertain fraction, regardless of the increase of accuracy in determining the initial condition. Although the mathematical conditions for riddling are quite difficult to verify directly, riddled basins can be characterized by scaling laws, whose critical exponents involve the computation of finite-time Lyapunov exponents. We described riddled basins for a coupled system of Lorenz-like systems, where there are two coexisting attractors thanks to the symmetries of its phase space. We obtained the scaling laws for the corresponding riddled basins of attraction and showed that the critical exponents for these laws can be predicted by a simple stochastic model even in this high-dimensional system. The distribution of finite-time Lyapunov exponents also allowed us to discuss the presence of an extreme form of shadowability breakdown inherent to riddled basins: unstable dimension variability. Due to the latter, computer-generated trajectories of dynamical systems are expected to be poorly shadowed by true chaotic trajectories. Our approach to analyzing this system is quite general and enabled us to verify the existence and some of the consequences of riddling and unstable dimension variability in a way that can be applied to a wide variety of systems of interest.

I. INTRODUCTION

Riddled basins of attraction occur in dynamical systems with more than one asymptotic state; it may be the case of two limited attractors, for example, or one of the basins can also refer to an unbounded (infinite) attractor.[1] The corresponding basins are said to be riddled if one of them is riddled with "holes" belonging to

Published under an exclusive license by AIP Publishing

the other, and these "holes" exist at arbitrarily fine scales. In terms of the final-state uncertainty, if a basin of attraction is riddled, any uncertainty in determining the initial condition can lead to complete uncertainty of the final state of the orbit.[2] This is an extreme fractal situation that has been observed in a variety of mathematical models as well as experiments.[3]

One of the mathematical conditions for riddled basins of attraction is the existence of a chaotic attractor in an invariant subspace of the system's phase space.[4] This invariant subspace can be a consequence of some symmetries in the phase space, or it can also be the synchronization manifold of coupled systems. An example of the former case was studied for the dynamics of a particle in a two-dimensional potential possessing such a symmetry,[5] leading to a two-dimensional subspace embedded in the four-dimensional phase space: one of the attractors comes from a Duffing-type oscillator, whereas the other is the attractor at infinity. The latter case can be represented by the synchronized manifold of some coupled map lattice, where the chaotic synchronized state is a solution of the coupled equations.[6]

The remaining mathematical conditions for riddling refer to the behavior of system dynamics along the directions transversal to the invariant subspace. The attractor in the subspace must be transversely stable, whereas there must also be a number of transversely unstable periodic orbits embedded in it. If the attractor becomes transversely unstable as a whole (the so-called blowout bifurcation), it transforms into a chaotic repeller, and riddling ceases to exist.[7,8]

Some of the above-mentioned mathematical conditions for riddling may be difficult to be verified directly with numerical accuracy. For example, the existence of transversely unstable periodic orbits can often be deduced more conveniently from the distribution of finite-time Lyapunov exponents.[9] In dynamical systems of practical interest, one often complements the Lyapunov analysis with the verification of scaling laws characteristic of riddled basins,[5,10] which consider (i) the probability of escaping from the vicinity of the attractor in the subspace, (ii) the final-state uncertainty with whom the initial conditions are determined. Such scaling laws, on their hand, have critical exponents that can be theoretically predicted based on a stochastic model proposed by Ott and collaborators,[11] which uses the properties of the finite-time transversal Lyapunov exponents. Since the Lyapunov exponents can be determined from typical chaotic orbits, with respect to the natural measure of the attractor, it is possible to verify the scaling laws for riddling and to compare the scaling exponent values with those predicted from the stochastic model.

In this paper, we are to exemplify this procedure for the determination of riddled basins in a model consisting of coupling two smoothed nonlinear versions of a Lorenz-like system recently proposed in Ref. 12; a study for the coupling of two Lorenz systems can be found in Ref. 13. Due to symmetries of the model equations, we found two coexisting attractors in the six-dimensional phase space: one corresponding to a chaotic synchronized state and the other to an anti-synchronized state. Since the former lies on an invariant manifold, we used the transversal Lyapunov exponent to determine one of the mathematical conditions for riddling, namely, that the attractor is transversely stable. The second condition (existence of transversely unstable periodic orbits) is demonstrated using periodic orbits obtained through a numerical method. We verify the scaling laws for riddling and compare the results with the theoretical values predicted by the stochastic model described in Ref. 11. We showed that this stochastic model can correctly predict the power-law exponents relevant to riddled basins even in our high-dimensional system.

This work is organized as follows: In Sec. II, we introduce the modified Lorenz-like system and describe its coupled version, characterizing the corresponding synchronization manifold and the two coexisting attractors to be analyzed. Section III is devoted to a description of the basins of attraction and the numerical results for the transversal Lyapunov exponents. Section IV considers the scaling laws for riddling and compares the numerically determined scaling exponents with the theoretical predictions of a stochastic model. In Sec. V, we discuss the concept of unstable dimension variability and its consequences for the system studied. Our conclusions are left to Sec. VI.

II. THE COUPLED LORENZ-LIKE SYSTEM

The Lorenz system is one of the cornerstones of nonlinear dynamics.[14] Although initially intended to be a simplified model of forced convection in the atmosphere, the Lorenz system has become a paradigmatic model for chaotic behavior, largely due to its distinctive "butterfly" attractor, which is both chaotic and fractal. Since its introduction in 1963, there have been many attempts to extend the model so as to exhibit more complicated attractors in phase space, e.g., without the limitation that the attractor be confined in the positive half-space with respect to the z-variable.[15]

In this work, we consider the following Lorenz-like model proposed by Elwakil and co-workers:[12]

$$\begin{aligned} \frac{d\tilde{x}}{dt} &= a\,(\tilde{y}-\tilde{x}),\\ \frac{d\tilde{y}}{dt} &= s\,k(\tilde{x})\tilde{z}+m,\\ \frac{d\tilde{z}}{dt} &= -s\,|\tilde{x}|+s, \end{aligned} \tag{1}$$

where $0 < a < 1$, m and $s = \pm 1$ are system parameters, and

$$k(\tilde{x}) = \begin{cases} 1 & \text{if } \tilde{x} \geq 0,\\ -1 & \text{if } \tilde{x} < 0 \end{cases} \tag{2}$$

replaces the cross product $\tilde{x}\tilde{y}$ in the original Lorenz equations, making this modified system a piecewise linear one, like Chua's equations,[16] for example. Hence, this can be considered a piecewise linear version of the Lorenz equations. An electronic circuit realization of this Lorenz-like system was proposed in Ref. 17. Subsequently, this system was further modified to exhibit more complicated butterfly-type attractors.[15]

The system in Eq. (1) exhibits a chaotic attractor for $a = 0.55$, $m = 0$, and $s = \pm 1$. There are two distinct chaotic attractors, depending on whether s is 1 or -1. In the original paper,[12] the authors considered the parameter s switching periodically in time between -1 and 1 so that both attractors appear as a four-winged

15 September 2024 03:59:26

Published under an exclusive license by AIP Publishing

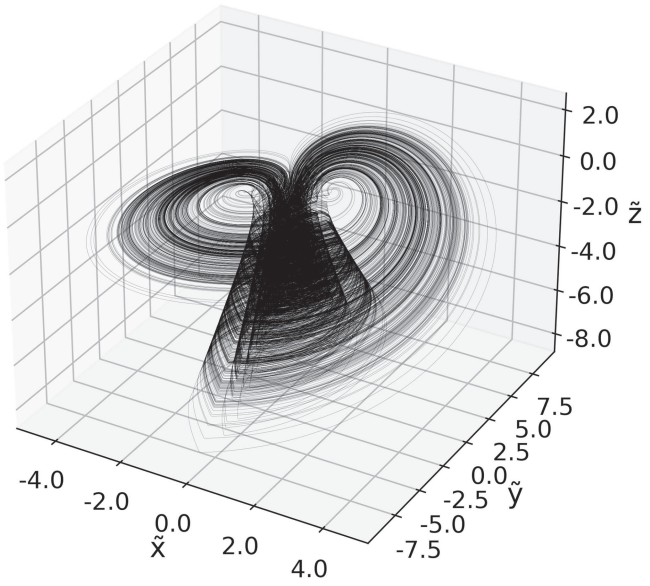


FIG. 1. Two-winged chaotic attractor for the modified Lorenz-like system in Eq. (3) with $a = 0.5$ and $c = 50$.

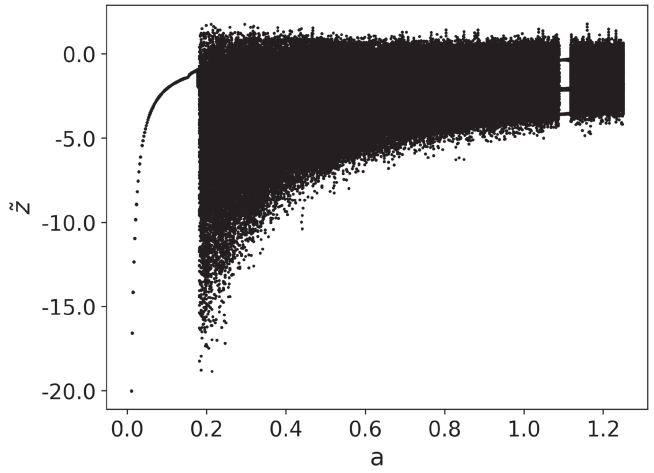


FIG. 2. Bifurcation diagram for possible values of $\tilde{z}(t_n)$ as a function of the parameter a, where $\tilde{z}(t_n)$ are the $\tilde{z}$-coordinates of the intersection of a trajectory with the plane $\tilde{x} = 0$, given by the map in Eq. (4).

butterfly attractor. We, on the other hand, will keep this parameter constant at $s = +1$. Furthermore, we set $m = 0$ for symmetry reasons, which will be significant when coupling these systems.

We consider in the present work a modified version of this Lorenz-like system by replacing the discontinuous function $k(\tilde{x})$ for the smoothed nonlinear function $\tanh(c\tilde{x})$, where $c > 1$. We did so because many interesting dynamics occur near $\tilde{x} = 0$, for which the original system is discontinuous, and this discontinuity affects the convergence of numerically computed Lyapunov exponents. Since for nonzero $\tilde{x}$, $\tanh(c\tilde{x})$ tends to $k(\tilde{x})$ as $c \to \infty$, the characteristic attractor is practically unchanged for relatively large values of c.

There follows that our modified version of the Lorenz-like system reads

$$\begin{aligned} \frac{d\tilde{x}}{dt} &= a\,(\tilde{y} - \tilde{x}), \\ \frac{d\tilde{y}}{dt} &= \tanh(c\tilde{x})\,\tilde{z}, \\ \frac{d\tilde{z}}{dt} &= -|\tilde{x}| + 1, \end{aligned} \tag{3}$$

where $c = 50$ and a is the only free parameter. This system has two fixed points located at $(\pm 1, \pm 1, 0)$. For $a \in [0, 1]$ and $\tanh c \approx 1$, these fixed points are linearly stable in the $\tilde{z}$-direction (with a real and negative eigenvalue for the Jacobian) and behave as unstable spirals in the $\tilde{x}\tilde{y}$ plane (two conjugate complex eigenvalues with a positive real part and a nonzero imaginary part). Figure 1 shows the two-winged butterfly chaotic attractor for $a = 0.5$.

We obtained numerically a Poincaré map by registering those trajectory points passing through the plane $\Pi = \{(\tilde{x}, \tilde{y}, \tilde{z}) \in \mathbb{R}^3 \mid \tilde{x} = 0\}$. If $\phi(t) = (\tilde{x}(t), \tilde{y}(t), \tilde{z}(t))$ is a solution of the system (3), for given initial conditions $(\tilde{x}_0, \tilde{y}_0, \tilde{z}_0)$, then we define a function $\mathcal{F} : \Pi \to \Pi$ and a map $v_{n+1} = \mathcal{F}(v_n)$ such that $v_n = (\tilde{y}(t_n), \tilde{z}(t_n))$ represents a point of the flux that crosses the plane Π at time t_n, that is, $\tilde{x}(t_n) = 0$. Then, let t_{n+1} be the smallest time $t > t_n$ such that $\phi(t) \in \Pi$. We define $\mathcal{F}$ and v_{n+1} as

$$v_{n+1} = \mathcal{F}(v_n) = (\tilde{y}(t_{n+1}), \tilde{z}(t_{n+1})). \tag{4}$$

A bifurcation diagram can be constructed by registering the $\tilde{z}(t_n)$ variables of this Poincaré map as a function of the tunable parameter a (Fig. 2). In order to obtain this diagram, we first integrated numerically the system equations for the smallest a chosen (in our case, $a_{\min} = 10^{-3}$) using an initial condition near the origin. Then, after computing all the possible values of $\tilde{z}(t_n)$ for this a, we take the last value $(\tilde{x}, \tilde{y}, \tilde{z})$ of the calculated solution, add a small perturbation to its state variables, and use this as an initial condition for the next value of a. Doing this process recursively for each a, the initial conditions are expected to always be near the attractor and within its basin of attraction. We observed that for $a \lesssim 0.18$, the attractor suddenly changes from periodic to chaotic and persists in this behavior up to small periodic windows within the parameter interval $a \in [0.18, 1.2]$.

Coupling two such modified Lorenz-like systems by their $\tilde{z}$ variables, with a coupling strength κ, results in the following model equations:

$$\begin{aligned} \frac{dx_i}{dt} &= a\,(y_i - x_i), \\ \frac{dy_i}{dt} &= z_i\,\tanh(cx_i), \\ \frac{dz_i}{dt} &= -|x_i| + 1 + \kappa\,(z_j - z_i), \end{aligned} \tag{5}$$

where $i, j = 1, 2$ and $j \neq i$. In order to examine the effects of coupling in greater detail, from now on, we will keep $a = 0.5$ fixed and only vary the coupling parameter κ.

15 September 2024 03:59:26

Published under an exclusive license by AIP Publishing

This system has a three-dimensional invariant synchronization manifold given by

$$\mathcal{M}_S = \{ (v_1, v_2) \in \mathbb{R}^6 \mid x_1 = x_2, y_1 = y_2, z_1 = z_2 \}, \tag{6}$$

where $v_1 = (x_1, y_1, z_1)$ and $v_2 = (x_2, y_2, z_2)$ since the system is invariant under the changes $v_1 \longleftrightarrow v_2$. When $v = (v_1, v_2) \in \mathcal{M}_S$, both v_1 and v_2 follow exactly the same dynamics given by Eq. (3), and each can converge to the two-winged chaotic attractor $\mathcal{A}$ in $\mathcal{M}_S$, displayed in Fig. 1, provided that v_1 (or v_2) is within its basin of attraction.

There are three transversal directions to the synchronization manifold. The dynamics along them can be more conveniently analyzed by transforming to the following coordinates:

$$\begin{aligned} x &= \tfrac{1}{2}(x_2 - x_1), & y &= \tfrac{1}{2}(y_2 - y_1), & z &= \tfrac{1}{2}(z_2 - z_1), \\ X &= \tfrac{1}{2}(x_2 + x_1), & Y &= \tfrac{1}{2}(y_2 + y_1), & Z &= \tfrac{1}{2}(z_2 + z_1). \end{aligned} \tag{7}$$

With them, the coupled model equation (5) is rewritten as

$$\begin{aligned} \frac{dx}{dt} &= a(-x + y), \\ \frac{dy}{dt} &= \frac{1}{2}\left\{(z - Z)\tanh(c(-x + X)) + (z + Z)\tanh(c(x + X))\right\}, \\ \frac{dz}{dt} &= \frac{1}{2}\left\{|x - X| - |x + X| - 4\kappa z\right\}, \\ \frac{dX}{dt} &= a(-X + Y), \\ \frac{dY}{dt} &= \frac{1}{2}\left\{(-z + Z)\tanh(c(-x + X)) + (z + Z)\tanh(c(x + X))\right\}, \\ \frac{dZ}{dt} &= \frac{1}{2}\left\{2 - |x - X| - |x + X|\right\}. \end{aligned} \tag{8}$$

For these transformed coordinates, the synchronization manifold $\mathcal{M}_S$ is given by $(x, y, z) = (0, 0, 0)$. There is another invariant manifold in the system subspace thanks to the invariance of the coupled model equations with respect to the transformation $(X, Y, z) \to (-X, -Y, -z)$. Hence, there is an anti-synchronized state given by $(X, Y, z) = (0, 0, 0)$, or $x_1 = -x_2$, $y_1 = -y_2$, and $z_1 = z_2$, lying on a corresponding invariant manifold $\mathcal{M}_A$ (or an anti-synchronization manifold),

$$\mathcal{M}_A = \{ (v_1, v_2) \in \mathbb{R}^6 \mid x_1 = -x_2, y_1 = -y_2, z_1 = z_2 \}. \tag{9}$$

Consequently, there is also a two-winged chaotic attractor $\mathcal{B}$ in $\mathcal{M}_A$ since for $(X, Y, z) = (0, 0, 0)$, the components (x, y, Z) follow the dynamics of Eq. (3).

For sufficiently large values of the coupling parameter κ, the system can present some form of chaos synchronization, with orbits converging either to $\mathcal{A}$ or to $\mathcal{B}$ according to the corresponding initial condition. However, if the coupling strength κ is too small, then the system will not converge to any of these two manifolds. Figure 3 shows, for two different values of κ, the distance from a trajectory to the synchronization manifold, $d_s(t) = [x^2(t) + y^2(t) + z^2(t)]^{1/2}$. If the coupling is relatively weak ($\kappa = 0.10$), a typical trajectory does not converge to $\mathcal{A}$ (nor to $\mathcal{B}$), a consequence of its being transversely unstable [Fig. 3(a)]. On the other hand, for stronger coupling ($\kappa = 0.15$), a trajectory (whose initial condition lies in the corresponding basin of attraction) rapidly converges to the synchronization manifold since $\mathcal{A}$ is transversely stable in this case [Fig. 3(b)].

In order to investigate the transversal dynamics of the orbits near the synchronized attractor, we can compute the Lyapunov spectrum for a chaotic orbit in the attractor. For a six-dimensional phase space of the coupled system, there are six Lyapunov exponents λ_i, $i = 1, 2, \ldots, 6$, of which the first three refer to directions lying on the synchronization manifold, whereas the remaining are for the directions transversal to this manifold. The most important of the latter is the maximal transversal exponent $\lambda_\perp \equiv \lambda_4$ (assuming that the transversal exponents are ordered) since its negativity implies that the synchronized state is on the average transversely attracting. To determine the whole Lyapunov spectrum, we can use the method described in Ref. 18.

Another method to obtain only the maximal transversal exponent is to use the so-called variational equations,[13] which utilizes the first-order dynamics of a transversal displacement from the synchronization manifold. These variational equations are derived by considering the dynamics of perturbations $(\delta x, \delta y, \delta z)$ in Eq. (8) and read

$$\begin{aligned} \frac{d}{dt}\delta x &= a(-\delta x + \delta y), \\ \frac{d}{dt}\delta y &= c\,Z\,\mathrm{sech}^2(cX)\,\delta x + \tanh(cX)\delta z, \\ \frac{d}{dt}\delta z &= -\mathrm{sign}(X)\,\delta x - 2\kappa\delta z, \\ \frac{dX}{dt} &= a(-X + Y), \\ \frac{dY}{dt} &= Z\tanh(cX), \\ \frac{dZ}{dt} &= 1 - |X|. \end{aligned} \tag{10}$$

The maximal transversal Lyapunov exponent $\lambda_\perp$ can be obtained by integrating the above equation with an initial displacement,

$$d_{\mathrm{lyap}}(t = 0) = \left\{(\delta x(0))^2 + (\delta y(0))^2 + (\delta z(0))^2\right\}^{1/2},$$

and is given by

$$\lambda_\perp = \lim_{t\to\infty} \frac{1}{t} \log\left(\frac{d_{\mathrm{lyap}}(t)}{d_{\mathrm{lyap}}(0)}\right), \tag{11}$$

taking the limit $d_{\mathrm{lyap}}(0) \to 0$. Since $d_{\mathrm{lyap}}(t)$ can increase exponentially, and in practice, we cannot numerically take the limit $d_{\mathrm{lyap}}(0) \to 0$, when evaluating the above expression, we used the technique described in Ref. 19, which consists of fixing a small time step Δt and calculating $d_{\mathrm{lyap}}(t)$ in steps.

The three largest values of the Lyapunov spectrum and the maximal transversal Lyapunov exponent, given by Eq. (11), for a trajectory in $\mathcal{A}$ are shown in Fig. 4. The orbits considered in these computations refer to the synchronized state (belonging to $\mathcal{M}_S$), but the results also hold for the anti-synchronized state in $\mathcal{M}_A$. The three largest Lyapunov exponents are depicted using different colors in Fig. 4: as expected, there is a positive Lyapunov exponent $\lambda_1 \approx$

15 September 2024 03:59:26

Published under an exclusive license by AIP Publishing

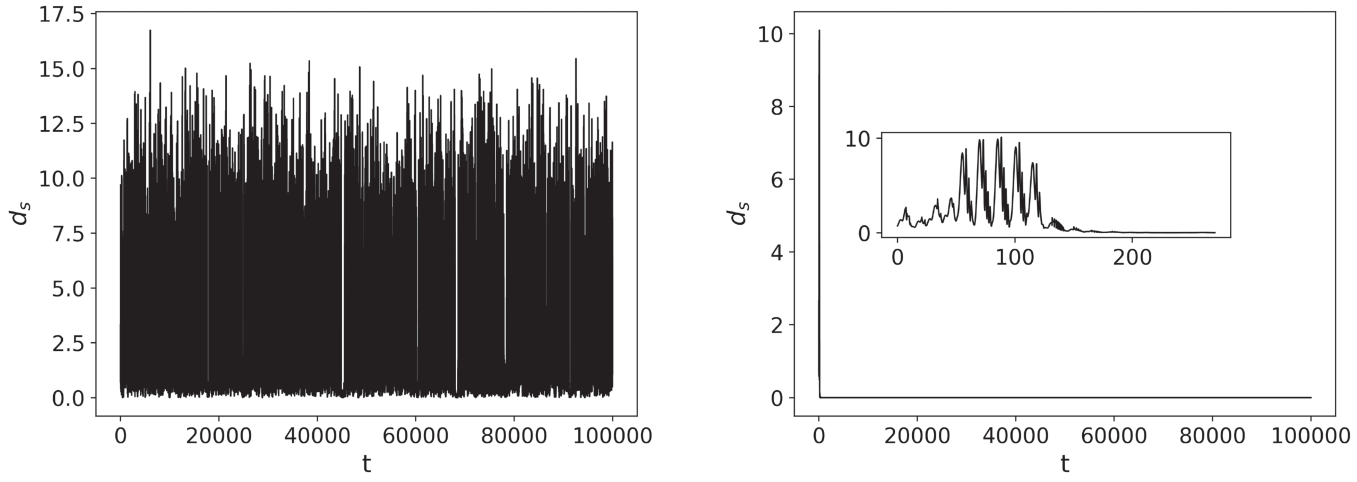


FIG. 3. Distance to the synchronization manifold d_s, as a function of time t, for two typical trajectories in the coupled system with initial conditions chosen randomly in $[-1, 1]^6$ for $a = 0.5$ and two values of κ. Figure (a) has $\kappa = 0.10$ and (b) has $\kappa = 0.15$. In the first case, the chaotic attractor in the synchronization manifold is transversely unstable so that orbits are not net attracted to it as $t \to \infty$. In contrast, in the second case, the attractor is transversely stable, and orbits within its basin can converge to it such that $d_s(t) \to 0$ as $t \to \infty$. The inset in (b) shows the transient before $d_s(t)$ converges.

0.14 for all considered values of the coupling strength κ associated with the chaotic orbit. In the interval $0 < \kappa < \kappa_c \approx 0.1208$, there is a second positive Lyapunov exponent, indicating hyperchaotic behavior, whereas the third largest exponent vanishes, as required for any continuous time system. For $\kappa > \kappa_c$, the third exponent becomes negative and the second vanishes, indicating that the synchronized attractor becomes transversely stable.

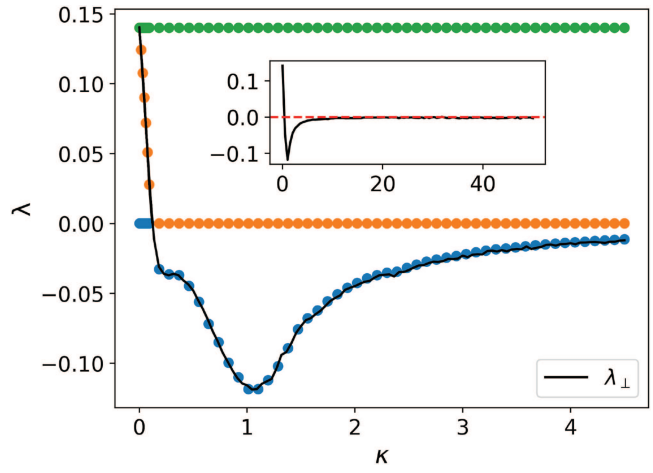


FIG. 4. Three largest values of the Lyapunov spectrum, colored dots, for $a = 0.5$, alongside the maximal transversal Lyapunov exponent $\lambda_\perp$ (black curve) for a chaotic orbit in the synchronization manifold as a function of the coupling strength κ. The inset illustrates the behavior of $\lambda_\perp$ in a larger interval of κ values.

In the same figure, we depicted using a black curve the transversal Lyapunov exponent $\lambda_\perp$ calculated by the variational equations, which is initially positive and crosses zero at κ_c, being negative for $\kappa > \kappa_c$. As a result, in the range $\kappa \in [0.0, 4.5]$, the chaotic attractor $\mathcal{A}$ in the synchronization manifold $\mathcal{M}_S$ is transversely stable for $\kappa > \kappa_c$ and is transversely unstable for $0 \leq \kappa < \kappa_c$. As we increase κ significantly from κ_c, $\lambda_\perp$ appears to approach zero from below without crossing it (at least for $\kappa < 50.0$, see the inset of Fig. 4).

III. RIDDLED BASINS OF ATTRACTION

Higher-dimensional dissipative systems are long known to have a complicated basin of attraction structure due to the presence of many coexisting attractors, each with its own basin that often displays fractal characteristics.[3] One can say, in general, that chaotic high-dimensional systems have intertwined basins of attraction, with a fractal boundary, resulting in difficulties for predicting their final-state behavior.

One of the outstanding features of a basin structure is the possible presence of riddled basins of attraction. The mathematical requirements for a dynamical system to possess riddled basins are the following:[1]

1. the system must have an invariant subspace $\mathcal{M}$ in its phase space, on which lies a chaotic attractor A;
2. there must be another attractor B with its corresponding basin of attraction;
3. the attractor A must be transversely stable, i.e., the maximal transversal Lyapunov exponent must be negative ($\lambda_\perp < 0$); and
4. there must be transversely unstable periodic orbits embedded in A.

15 September 2024 03:59:26

Published under an exclusive license by AIP Publishing

Once these conditions are fulfilled, the basin of attraction of A can be riddled with (measure-theoretical) holes belonging to the basin of the second attractor B.[3] If the basin of B is also riddled with holes belonging to the basin of A, then both basins are said to be intermingled.[20]

Riddling can be viewed as an extreme form of fractal behavior because it occurs in all scales: every disk (representing an ε-neighborhood) centered at a point belonging to the basin of A contains a nonzero fraction of points belonging to the basin of the B, no matter how small ε may be.[21] Given that ε may represent the uncertainty with which an initial condition is determined, in riddled basins, no decrease of ε is going to improve the final-state predictability of the system, i.e., any initial condition is ε-uncertain, regardless of ε being large or small.

In our coupled system, conditions 1 and 2 for riddling are fulfilled by assigning A and B to be the synchronized and anti-synchronized attractors, respectively. Condition 3, as depicted in Fig. 4, is fulfilled for $\kappa > \kappa_c \approx 0.1208$. We will discuss condition 4 later. Meanwhile, plots of the basins of attraction, using values of κ for which the synchronized attractor in $\mathcal{M}_S$ is transversely stable, suggest that the basin of attraction for the synchronized state appears to be riddled.

In Fig. 5, we consider a two-dimensional cross section of the phase space by taking fixed values $x_1 = x_2 = 1.0$ and $y_1 = y_2 = 1.0$, while varying z_1 and z_2. The black (respectively white) pixels represent initial conditions generating trajectories that converge to the anti-synchronized (respectively synchronized) attractor. For these values of x and y, the synchronized attractor looks almost dense in the region $z \in [-6, 1]$ such that we can assume that the line $z_1 = z_2$ in the range $[-6, 1]$ is predominantly contained within the chaotic attractor in $\mathcal{M}_S$. We note the characteristic tongues of points (formed by black pixels) that diverge from $\mathcal{M}_S$, which is a typical feature of riddled basins of attraction.[22,23]

Since the origin of $\mathbb{R}^6$ in the new coordinates, given by Eq. (7), lies on both invariant manifolds, another two-dimensional cross section of the basins can be seen by fixing $y_1 = \pm y_2 = 0.0$ and $z_1 = z_2 = -2.0$, while varying x_1 and x_2. This setup allows us to visualize the riddled basins of both the synchronized and anti-synchronized attractors. This is illustrated in Fig. 6, which shows the basins of attraction for the attractors in the synchronization (white pixels) and anti-synchronization (black pixels) manifold, represented by the blue and the red lines in the plot that intersect at the origin. Consequently, the black and white basins are intermingled since the basin of one is riddled with holes of the other and vice versa.

In our numerical explorations of the coupled system, we did not observe other coexisting attractors or an unbounded attractor (at infinity). Since, in principle, we cannot rule out these possibilities, we can regard one of the basins (e.g., the white one) as the union of all the possibly other existing basins. This does not invalidate, however, any of the conclusions we have obtained.

Now, we discuss Condition 4 for riddling, namely, the existence of periodic orbits embedded in the chaotic attractor such that there are both transversely stable and unstable ones. The presence of the stable orbits is expected since the chaotic orbit can be approximated by periodic orbits of arbitrarily large periods. The existence of transversely unstable periodic orbits, however, is an essential property for

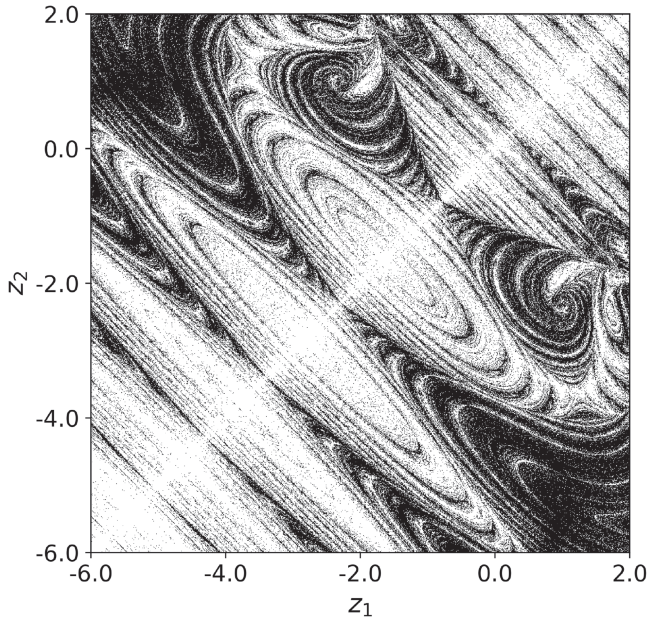


FIG. 5. Two-dimensional cross section of the basins of attraction for the two-winged chaotic attractor in $\mathcal{M}_S$ (pixels in white) and in $\mathcal{M}_A$ (pixels in black) for $\kappa = 0.41$. For this cross section of the phase space, we considered $x_1 = x_2 = 1.0$ and $y_1 = y_2 = 1.0$.

riddling. This is because although the set of unstable periodic orbits is of zero natural measure in the invariant subspace of $\mathcal{A}$, every one of these orbits creates, by continuity, a region of a positive Lebesgue measure in the phase space, arbitrarily close to $\mathcal{A}$, that is locally repelling and that can be in the basin of another attractor. This is the mechanism by which the tongue-like regions in the basins of attraction are created.[11,22,23] Furthermore, if the set of periodic orbits is dense in the attractor, these repelling regions will appear in any neighborhood of the attractor.

In order to verify the existence of transversely unstable periodic orbits in the synchronized chaotic attractor $\mathcal{A}$, we calculated some of them using the Newton–Raphson–Mees method with a damping coefficient, described at Ref. 24, and briefly explained in the Appendix. Figure 7 shows some examples, in orange, of periodic orbits embedded in the synchronized attractor. The fixed points $(\pm 1, \pm 1, 0)$ are in red, and the gray curve is part of the chaotic attractor. Similarly to what happens in the Lorenz attractor, these periodic orbits appear to always rotate around the two symmetric fixed points.[25] However, in our system, the periodic orbits may also rotate a number of times around the z axis so that the symbolic dynamics of this system is more complicated and seemingly cannot be described by just two symbols, as is the case for the classical Lorenz attractor.[26] Table I shows the values of some of the initial conditions (x, y, z) associated with periodic orbits, as well as their periods T, that were obtained by this method.

Figures 8(a) and 8(b) show the maximal transversal Lyapunov exponent $\lambda_\perp$ for the periodic orbits in Table I, labeled by their approximate periods T, as a function of κ. In Fig. 8(a), the coupling parameters are chosen to be near the blowout bifurcation,

15 September 2024 03:59:26

Published under an exclusive license by AIP Publishing

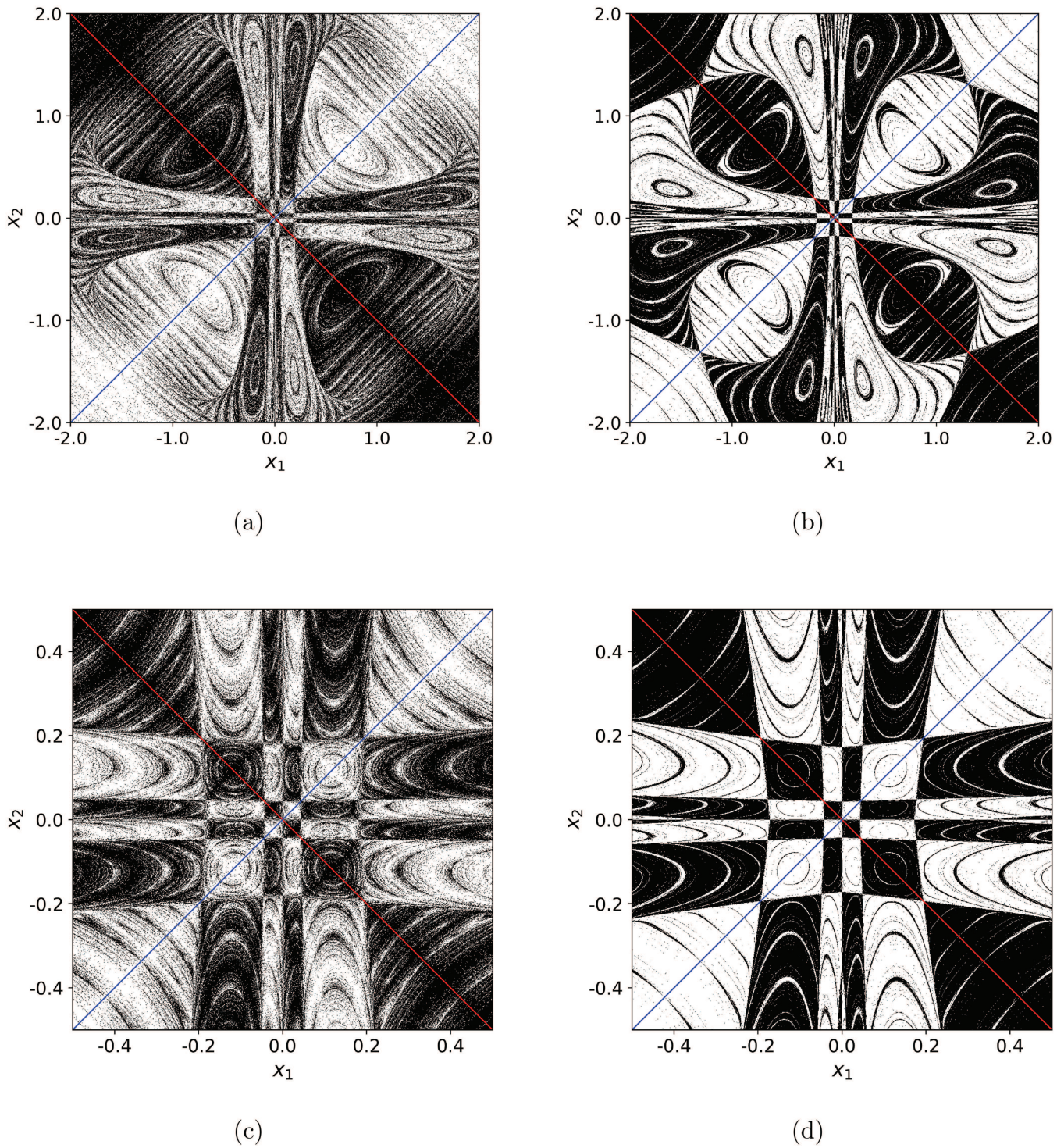


FIG. 6. Two-dimensional cross sections of the basins of attraction for the attractor in $\mathcal{M}_S$ (pixels in white) and in $\mathcal{M}_A$ (pixels in black) for $\kappa = 0.3$ in panel (a) and $\kappa = 1.0$ in (b). Panels (c) and (d) are magnifications of (a) and (b), respectively. For these cross sections of the phase space, we fixed $y_1 = \pm y_2 = 0.0$ and $z_1 = z_2 = -2.0$. The blue line is in $\mathcal{M}_S$, while the red line is in $\mathcal{M}_A$.

15 September 2024 03:59:26

Published under an exclusive license by AIP Publishing

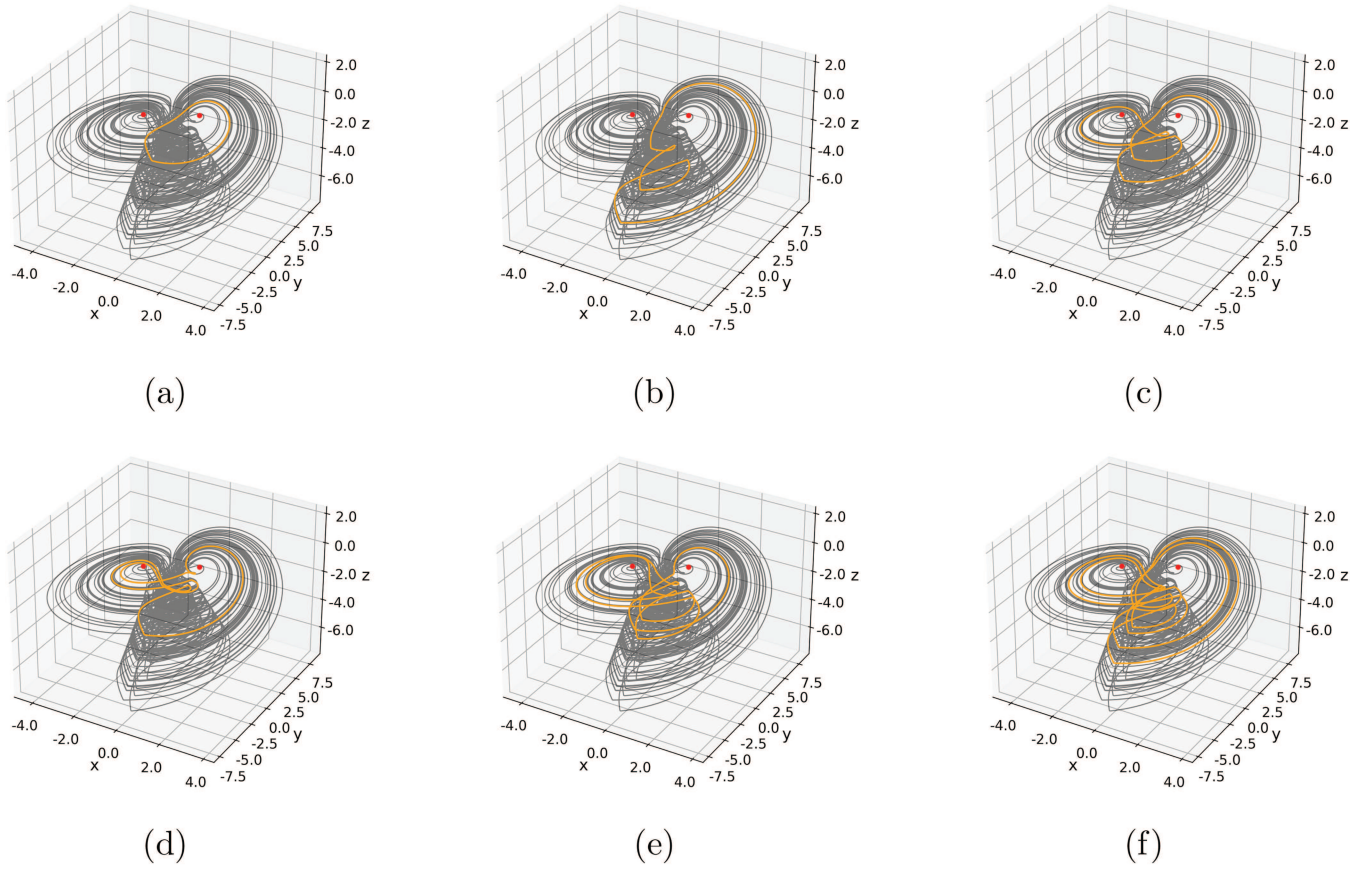


FIG. 7. Some periodic orbits (in orange) embedded in the synchronized chaotic attractor (in gray) with approximate periods $T =$ (a) 10.973, (b) 16.406, (c) 25.657, (d) 36.478, (e) 42.501, and (f) 56.899 (see also Table I).

while in Fig. 8(b), they are in a wider range $\kappa \in [0, 10.0]$. Before the blowout bifurcation, some of the periodic orbits turn transversely stable so that at the bifurcation, and in fact for all values of κ in the interval $[\kappa_c, 10.0]$, there coexist transversely stable and unstable periodic orbits. Therefore, we can conclude that for κ in this interval, all four conditions for riddling are fulfilled.

IV. SCALING LAWS FOR RIDDLED BASINS

In addition to the direct verification of the mathematical conditions for riddling, as we did in Sec. III, it is also possible to characterize riddled basins using scaling laws based on numerical experiments. Moreover, the scaling exponents can be estimated theoretically using models based on stochastic processes related to the finite-time Lyapunov exponents.

In riddled basins, we typically see two types of power-law behaviors. The first is related to the fraction $P^\star(y_0)$ of initial points that distance y_0 from one attractor (where y_0 is considered small) and do not converge to it.[5] For our coupled system, since the attractor lies in the synchronization manifold, y_0 stands for the Euclidean

TABLE I. Initial conditions (x, y, z) associated with each periodic orbit in the synchronized attractor used in Fig. 8, along with their approximate periods T.

x	y	z	T
−0.386 740 8	0.796 981 3	−1.000 670 2	10.973 236 7
−0.145 779 2	−1.650 969 6	−1.123 420 4	13.230 735 5
−0.214 938 5	3.074 200 1	−3.800 562 1	15.565 269 9
−1.559 622 6	−1.485 139 6	−0.658 700 8	15.745 696 0
0.304 249 6	−2.207 631 5	−4.135 843 2	16.405 654 3
−3.191 230 2	−5.760 272 3	0.374 737 3	19.579 149 1
0.376 760 4	−3.352 240 6	−3.107 182 9	25.657 343 3
−0.194 289 1	5.817 737 3	−5.207 276 9	30.880 099 2
1.312 358 7	0.684 501 4	−0.940 321 4	31.725 423 8
−0.146 768 6	1.795 068 6	−3.149 611 4	32.063 945 7
−0.559 638 6	−1.082 786 7	0.387 384 4	36.477 903 1
0.488 174 5	0.580 004 8	0.235 696 0	42.500 928 7
−0.141 450 9	−1.640 916 1	−1.734 370 4	56.899 342 3
0.269 002 1	4.387 234 7	−3.740 458 9	62.526 780 3

15 September 2024 03:59:26

Published under an exclusive license by AIP Publishing

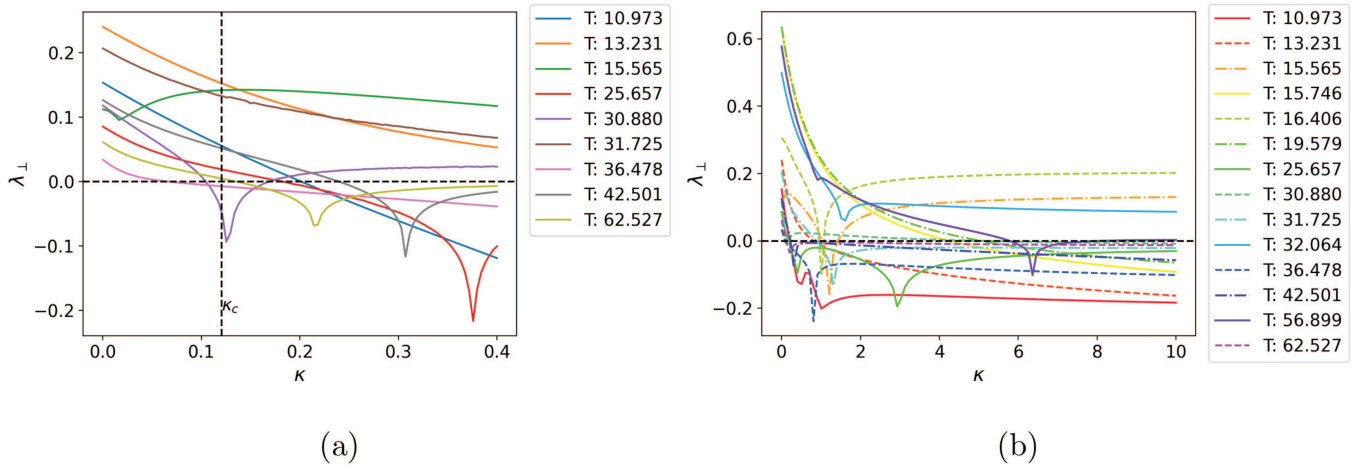


FIG. 8. Maximal transversal Lyapunov exponent $\lambda_\perp$ as a function of the coupling strength κ for unstable periodic orbits of different periods T embedded in the synchronized attractor. (a) Shows κ values near κ_c, while (b) covers a larger interval of κ values.

distance between the trajectory and the three-dimensional subspace $\mathcal{M}_s$.

Another scaling law holds for the so-called uncertain fraction of initial conditions $p(\varepsilon)$,[2,27] where $\varepsilon > 0$ is the uncertainty radius, which is calculated as follows: we take a point P_1 randomly that distances y_0 from the attractor, transversely from the invariant subspace. Subsequently, another point P_2 that also distances y_0 from the attractor is chosen such that the distance between P_1 and P_2 is uniformly distributed in the interval $[-\varepsilon, \varepsilon]$. Then, $p(\varepsilon)$ is the fraction of these initial conditions that results in P_1 and P_2 converging to different attractors. In this sense, $p(\varepsilon)$ can be seen as a measure of the uncertainty of the asymptotic behavior of a point that distances y_0 from the attractor as a function of the uncertainty in the initial condition ε.

For y_0 and ε small enough, we expect that both $P^\star(y_0)$ and $p(\varepsilon)$ exhibit power-law behavior for riddled basins[3,11] so that

$$\begin{aligned} P^\star(y_0) &\sim y_0^\eta, \\ p(\varepsilon) &\sim \varepsilon^\alpha, \end{aligned} \tag{12}$$

where η and α are scaling exponents. The latter scaling law is often assigned to fractal basins of attraction, where the uncertainty exponent is given by $\alpha = D_0 - d_0$, with D_0 representing the phase space dimension and d_0 the box-counting (capacity) dimension of the fractal basin boundary.[28] Regarding riddling as an extreme form of fractal behavior, the basin boundaries are so complicated that their dimension approaches that of the phase space itself; i.e., riddled basins are characterized by an almost vanishing scaling exponent α. We remark, however, that $\alpha \approx 0$ is not, strictly speaking, a definition of riddling since the latter has more stringent mathematical requirements, e.g., the existence of an invariant subspace. If this does not happen, for example, $\alpha \approx 0$ characterizes intertwined basins, but not necessarily riddling.[29]

Figure 9(a) shows for various values of κ and $a = 0.5$ the dependence of $P^\star(y_0)$ with y_0, over five orders of magnitude, for the basin of the synchronized attractor. The dashed lines are least square fits for each value of coupling strength κ portrayed. For all of them, we observed scaling behavior compatible with Eq. (12), with distinct exponents. Figure 9(b) similarly depicts $p(\varepsilon)$ as a function of ε over the same range, with fixed $y_0 = 10^{-2}$. In all cases, we observed that the power-law represents well the numerical data. The slopes of most of the least squares fits are small enough to indicate that $\alpha \approx 0$. This suggests that the basin structure is so complex that the fractal basin boundary dimension is close to the phase space dimension itself. Moreover, practically, no improvement in the accuracy of determining the initial condition would result in a substantial decrease in the uncertain fraction, which is a hallmark of riddled basins.

The scaling laws for riddled basins and the corresponding values of their exponents can be predicted theoretically on the basis of a stochastic process involving the dynamics in the directions transversal to the synchronization manifold. The model proposed by Ott, Alexander, Kai, Sommerer, and Yorke (hereafter called the OAKSY model)[11] is based on the properties of the finite-time transversal Lyapunov exponents $\tilde{\lambda}_\perp(\tau)$, which are defined in the same way as in Eq. (11), but when a finite time τ is taken.[30] Whereas $\tilde{\lambda}_\perp(\tau)$ depends, in general, from the initial condition, its infinite-time limit

$$\lambda_\perp = \lim_{\tau\to\infty} \tilde{\lambda}_\perp(\tau) \tag{13}$$

does not. For a chaotic orbit, this means that the time-τ transversal Lyapunov exponent can be treated approximately as a continuous random variable with a given probability distribution function $\mathcal{P}(\tilde{\lambda}_\perp(\tau))$.[31]

For statistical purposes, in order to calculate the distribution, we select a large number of randomly chosen initial conditions according to the attractor measure. However, using ergodicity, we can obtain the same effect by dividing a long-duration chaotic trajectory into a large number of short trajectory segments of duration τ. We then compute the corresponding finite-time maximal

15 September 2024 03:59:26

Published under an exclusive license by AIP Publishing

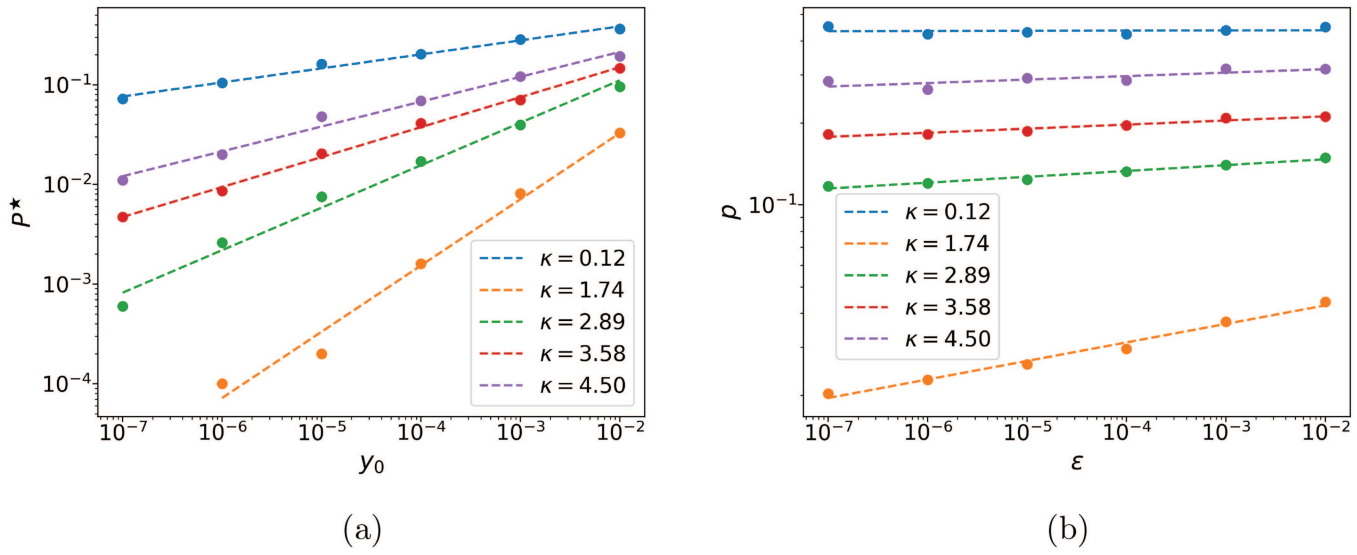


FIG. 9. (a) Fraction of initial conditions $P^\star$ that diverge from the synchronization manifold given that the initial condition distances y_0 from it. (b) Uncertain fraction p of initial conditions that distance $y_0 = 10^{-2}$ from the synchronization manifold as a function of the uncertainty radius ε. The dashed lines are linear fits on a logarithmic scale.

transversal exponents, obtaining a numerical approximation for $\mathcal{P}(\tilde{\lambda}_\perp(\tau))$.

Figure 10 shows the distribution of finite-time $\tau = 200$ transversal Lyapunov exponents for the attractor in $\mathcal{M}_S$ for three values of the coupling strength κ. The dashed lines also show the corresponding Gaussian distributions with the same mean and variance of the numerically obtained distribution. In all these cases, the distribution of finite-time Lyapunov exponents is well-represented by Gaussian distributions. This Gaussian-like nature of the distributions contributes to the validity of the OAKSY model, the agreement being better as close as we are to the blowout bifurcation.[3]

The log-distances $\tilde{d} = \log d_s$ to the synchronization manifold evolve, after a finite time τ, as

$$\log|\tilde{d}(\tau)| \sim \log|\tilde{d}(0)| + \tau\,\tilde{\lambda}_\perp(\tau),$$

which can be approximately regarded as a stochastic process, provided we neglect the time correlations that come from the fact that the original dynamical system is deterministic, as reflected in the distribution of the finite-time transversal Lyapunov exponents. In the OAKSY model, a diffusion equation is obtained and solved for the probability distribution of the log-distances. From this analysis, the diffusion coefficient D is related to the variance $\sigma^2(\tau)$ of the distribution of time-τ transversal Lyapunov exponents by[11]

$$D = \lim_{\tau\to\infty} \frac{\tau\sigma^2(\tau)}{2}. \tag{14}$$

This relation is illustrated in Fig. 11, where we plot the variance as a function of the time τ for different values of κ in a logarithmic scale alongside least squares linear fits. From Eq. (14), the diffusion coefficient is obtained from the intercepts of these fits. The scaling laws for riddled basins can be obtained by solving the diffusion equation, using Laplace transforms, with specified boundary conditions (see Ref. 11 for details). From these solutions, it follows that the scaling exponents are related to the parameters of the diffusion

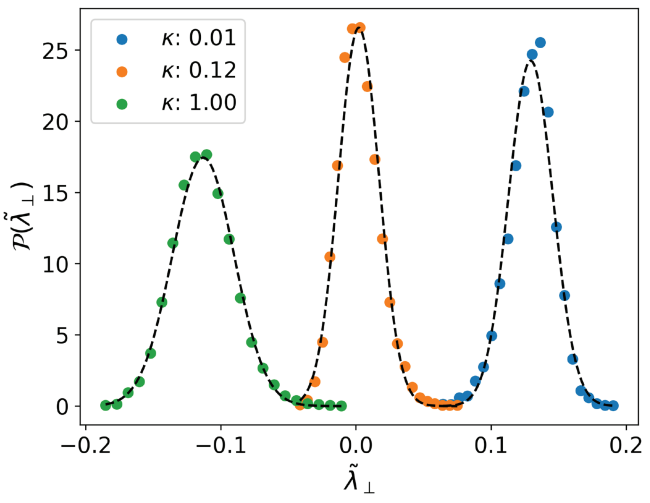


FIG. 10. Probability distribution functions $\mathcal{P}(\tilde{\lambda}_\perp(\tau))$ for the finite-time $\tau = 200$ transversal Lyapunov exponents in the synchronization manifold for three coupling parameters κ. The dashed curves are Gaussian distributions with the same mean and variance as the calculated distributions.

15 September 2024 03:59:26

Published under an exclusive license by AIP Publishing

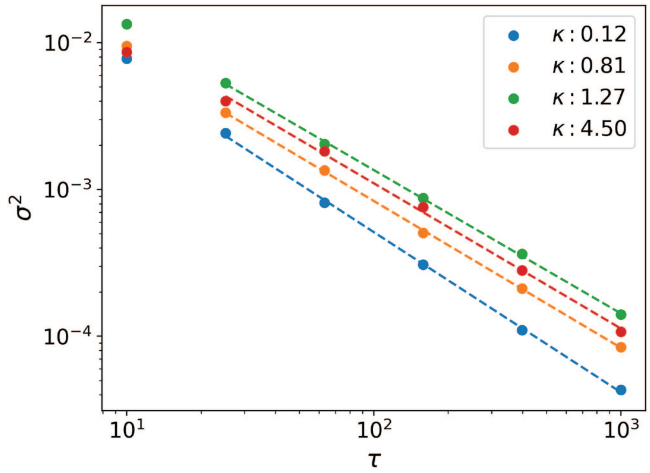


FIG. 11. Variance σ^2 of the distribution of time-τ transversal Lyapunov exponents for the synchronized attractor as a function of τ alongside linear fits in a log–log scale for different values of the coupling parameter κ.

approximation by

$$\eta = \frac{|\lambda_\perp|}{D}, \qquad \alpha = \frac{\lambda_\perp^2}{4D\lambda_\parallel}, \tag{15}$$

where $\lambda_\perp$ and $\lambda_\parallel$ are, respectively, the (infinite-time) largest transversal and parallel (with respect to the invariant subspace) Lyapunov exponents for an orbit in the synchronization manifold. Figures 12(a) and 12(b) show the values of these parameters calculated from (i) in orange, the slopes of least squares fits of numerically obtained trajectories (as in Fig. 9) and (ii) in blue, the stochastic model using the finite-time transversal Lyapunov exponent distribution and Eq. (15).

The model appears to correctly predict the scaling exponents in its range of validity, that is, when $\lambda_\perp$ is negative and close to zero and, hence, when the system is close to a blowout bifurcation. In our system, this occurs both near κ_c and for large values of κ, as can be seen in Fig. 4. There are intervals of κ, however, where this agreement is poor, meaning that the stochastic hypothesis underlying the model does not fully hold in those situations. In those intervals, the correlations among finite-time segments of a long chaotic trajectory may not be taken as uncorrelated, and the deterministic content of the corresponding probability distribution function turns more difficult to compare the results with those from a pure stochastic model. In this sense, the "worst" values are those with κ near the unity, where both scaling law exponents display significant deviations from the theoretical predictions.

V. UNSTABLE DIMENSION VARIABILITY

A hyperbolic chaotic invariant set is such that the tangent space is continuously splitted into unstable and stable manifolds of dimensions d^u and d^s, respectively. Moreover, these manifolds must cross transversely at each point. These conditions make it possible to generate Markov partitions, which guarantees many important dynamical properties. One of them is the shadowing of chaotic orbits.[32]

Due to roundoff errors and inaccuracies related to the finite-precision of computer arithmetics, numerical trajectories of chaotic systems are, in fact, pseudo-trajectories. In chaotic systems, this would be a great source of problems due to the extreme sensibility to initial conditions exhibited by such systems. However, under some circumstances, a numerically generated pseudo-trajectory can be shadowed (i.e., closely followed) by a true chaotic trajectory for some time interval t_s.[33]

For hyperbolic systems, it has been proved that t_s is infinite (Anosov shadowing lemma);[32,34] i.e., a chaotic pseudo-trajectory can be shadowed by a true one for an arbitrarily long time. This means that the computed orbit may not be that sought for, but that there is a *bona fide* chaotic orbit that stays close to the computed orbit. Hyperbolic systems are relatively rare and restricted to a few idealized examples. Most systems of interest are non-hyperbolic since they present a variety of factors (such as bifurcations and crises) that violate the mathematical requirements for hyperbolicity. One such example is the well-known Hénon map, whose shadowability properties have been recently investigated by Professor Jason A. C. Gallas.[35]

The presence of crises, for example, in which the chaotic attractor undergoes a sudden change as a system parameter is varied, represents a source of non-hyperbolic behavior, since crises are typically characterized by homoclinic or heteroclinic tangencies of the invariant manifold.[36] Such tangencies violate the required transversality of the manifold intersections. It turns out that even in these cases, it is possible to assign to the average of shadowing times $\langle t_s \rangle \sim \delta^{-h}$, where δ is the one-step error of pseudo-trajectories and h is a scaling exponent.[37] Since t_s can still be large, depending on the situation, we are facing here a mild obstruction to shadowability of chaotic trajectories.[23]

There is another more severe obstruction to shadowability that occurs in strongly non-hyperbolic systems, which exhibit the so-called *unstable dimension variability* or UDV for short.[31] In such cases, the dimensions of the stable and unstable manifolds (d^s and d^u) vary along the invariant chaotic set, violating the requirement of continuous splitting of the tangent space.

Non-hyperbolic systems with UDV were first described by Abraham and Smale,[38] in the context of a diffeomorphism. The first example of a dynamical system of physical interest displaying UDV was described in Ref. 39: the periodically kicked double rotor, which is described by a four-dimensional dissipative map. It has been found that UDV for this system is triggered by an interior crisis.[40] Another example is a torus map with dense sets of saddles and repellers,[31] which is linked to the notion of hetero-chaos.[41]

Unstable dimension variability typically occurs in coupled chaotic systems.[9,42] The existence of a synchronization manifold provides an invariant chaotic set where UDV can be found for certain values of the coupling constant, as shown by lattices of coupled Hénon and Ikeda maps.[43]

The direct verification of UDV requires identifying unstable periodic orbits embedded in the chaotic invariant set with a varying

15 September 2024 03:59:26

Published under an exclusive license by AIP Publishing

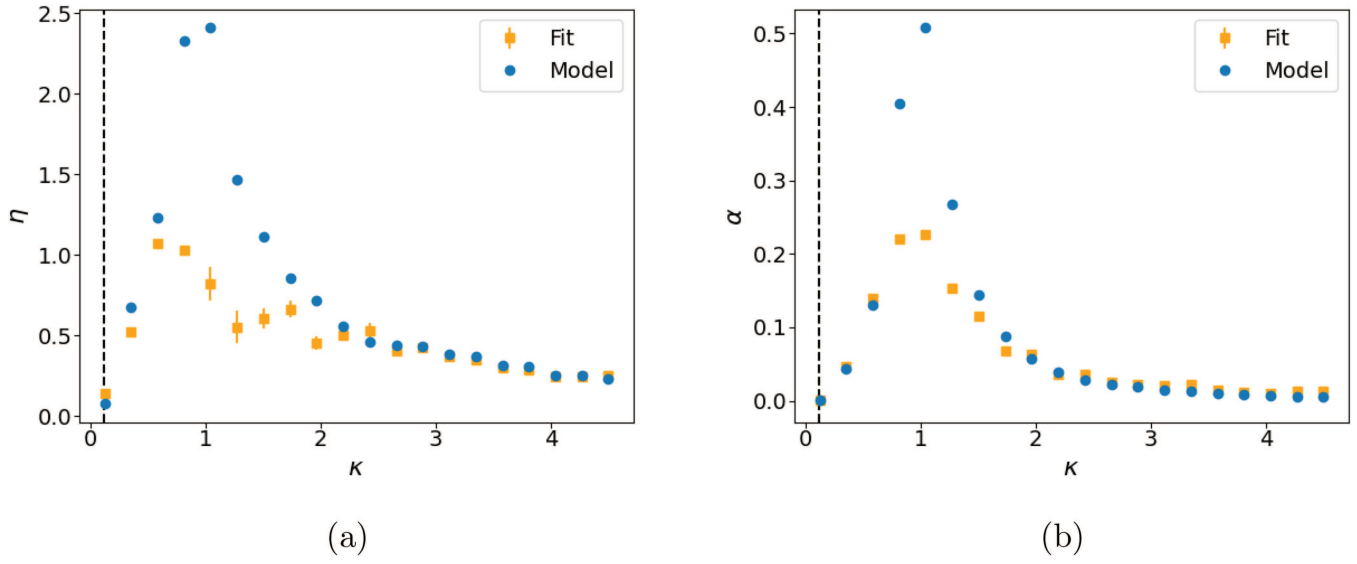


FIG. 12. Values of the power-law exponents related to the synchronized attractor basin: (a) η and (b) α. In orange are the values calculated directly by the fit of numerical orbits, as illustrated in Fig. 9, while in blue are the expected values from the OAKSY model, given by Eq. (15). The black vertical line indicates the critical value for κ associated with the blowout bifurcation.

number of unstable directions. This is feasible for simple systems, in which the phase space is simple enough for this investigation.[44,45] On the other hand, such an approach would be quite difficult for dynamical systems of physical interest due to the high dimensionality of the phase space.

A simpler way to characterize UDV relies on the properties of the finite-time Lyapunov exponents. The relative abundance of periodic orbits with different numbers of unstable directions can be evaluated by computing the distribution of finite-time Lyapunov exponents.[23] More precisely, we consider the maximal (closest to zero) finite-time Lyapunov exponent along the transversal direction $\tilde{\lambda}_\perp(\tau)$, as defined in Eq. (11). In systems with UDV, the existence of different numbers of an unstable direction implies that the time-τ transversal Lyapunov exponents fluctuate around zero.[46]

In order to understand qualitatively the reason for this association, let us consider an initial condition off but very close to the attractor lying in the synchronization manifold. In the context of high-dimensional dynamical systems, we can loosely speak of "saddles" and "repellers" with different numbers of unstable directions: if saddles have d^u unstable directions, then repellers will have $d^u + 1$ of them. The trajectory generated from this initial condition visits ϵ-neighborhoods of saddles and repellers for any ϵ, no matter how small. Consequently, there will be trajectory segments of duration τ for which the trajectory is transversely attracting on average and other segments where it is transversely repelling on average. Hence, the maximal time-τ transversal Lyapunov exponents will have both positive and negative values.

Let us consider, thus, a chaotic trajectory generated from such an initial condition (off but very close to the synchronization manifold). The presence of UDV is equivalent to the requirement that the positive fraction of such exponents

$$F(\lambda_\perp(\tau)) = \int_0^\infty d\tilde{\lambda}_\perp(\tau)\, P(\tilde{\lambda}_\perp(\tau)) \tag{16}$$

is such that $0 < F < 1$. If $F = 0$, all exponents are negative (indicating that only saddles are present), whereas $F = 1$ implies only positive exponents, indicating the exclusive presence of repellers. These limit situations do not characterize UDV.

Using as a tunable parameter the coupling constant κ, we can, thus, determine the onset of UDV as the values of κ for which F is different from zero and unity. Moreover, the point where the UDV is maximal is such that half of the exponents are positive, i.e., a fraction of $F = 1/2$. In such a situation, there is an equal relative number of saddles and repellers in the chaotic invariant set. In order to understand why at this point the UDV is maximal, we can make use of the results of a stochastic model, similar to the OAKSY model, that has been applied to estimate the shadowing exponents h of the average shadowing times $\langle t_s \rangle \sim \delta^{-h}$ as[33]

$$h = \frac{2\mu}{\sigma^2}, \tag{17}$$

where μ and σ^2 are, respectively, the average and variance of the distribution of the maximal transversal finite-time Lyapunov exponents. Supposing that the probability distribution function of the latter is unimodal and centered at $\lambda_\perp$, as suggested by Fig. 10, at the point where $F = 0.5$, we have $\mu \approx 0$ such that $h \approx 0$ and the average shadowing time $\langle t_s \rangle$ is minimum.

The variation of this fraction with the coupling coefficient κ is shown in Fig. 13 for different values of τ. For small τ, it turns out that F is nonzero for all values of κ, suggesting that UDV is a robust phenomenon in our coupled system. However, larger values of τ

15 September 2024 03:59:26

Published under an exclusive license by AIP Publishing

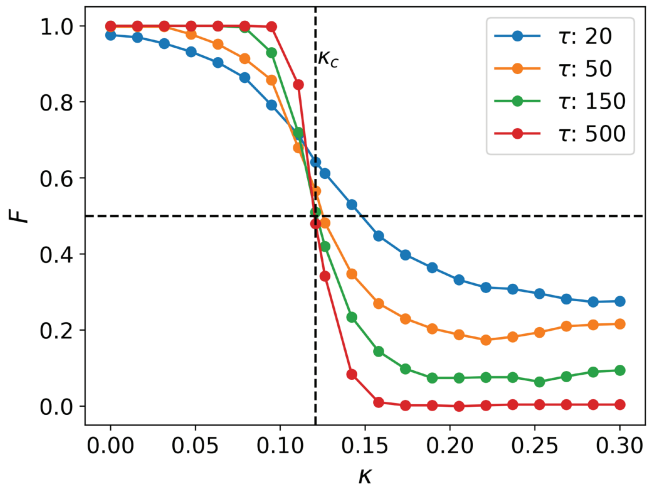


FIG. 13. Fraction F of positive finite-time τ transversal Lyapunov exponents for the chaotic attractor in the synchronization manifold as a function of the coupling parameter κ. The vertical black line indicates the critical value of κ_c, and the horizontal line is $F = 0.5$.

indicate that the onset of UDV occurs at $\kappa \approx 0.10$ and ceases to exist at $\kappa \approx 0.15$, these values being dependent on τ. Moreover, the value of $\kappa = \kappa^*$ for which $F = 1/2$ (maximum UDV) also depends on τ: for $\tau = 20$, we have $\kappa^* \approx 0.15$, decreasing its value with τ, whereas for $\tau \geq 150$, it follows that $\kappa^* \approx \kappa_c$, which is just the point where there occurs a blowout bifurcation (indicated as a dashed vertical line in Fig. 13).

Hence, for large τ, when $\kappa < \kappa_c$, the attractor in the synchronization manifold is transversely unstable and $F(\lambda_\perp) > 0.5$, while for $\kappa > \kappa_c$, we have $F(\lambda_\perp) < 0.5$ and the attractor is transversely stable. Thus, there is a connection between the blowout bifurcation and the relative number of transversely stable/unstable periodic orbits in the large-τ limit. Therefore, using the properties of the finite-time transversal Lyapunov exponents, we have numerical evidence for the presence of UDV in our coupled system for κ near κ_c. Indeed, we have shown in Secs. II–III that for any κ in the range $[\kappa_c, 10.0]$, there are both transversely stable and unstable periodic orbits embedded in the synchronized and anti-synchronized chaotic attractors (see Fig. 8).

VI. CONCLUSIONS

Riddled basins of attraction occur when there is multi-stability and a transversely stable chaotic attractor, in the weak Milnor sense, on an invariant subspace with unstable periodic orbits embedded in it. Therefore, the loss of transversal stability in this case is associated with a blowout bifurcation, which destroys these basins. In this work, we investigated the riddled basins, the blowout bifurcation, and the presence of unstable dimension variability for the coupling of two identical chaotic continuous systems, each having the same symmetries of the Lorenz attractor. Because of these symmetries, there are two chaotic attractors, one associated with a synchronization manifold and another with an anti-synchronization manifold. We verified that their respective basins of attraction can be riddled basins for a wide range of coupling parameters. In particular, each of the basins is riddled with "holes" belonging to the other such that the basins are actually intermingled.

These conclusions were first drawn based on the numerical evidence that for a coupling parameter κ greater than a critical value, all the mathematical conditions for riddling are fulfilled. This includes the presence of transversely unstable periodic orbits, some of which were numerically obtained using the Newton–Raphson–Mees method.

Another procedure we used to characterize riddled basins was to verify their scaling behavior. The first scaling law involves determining the fraction of initial conditions that diverge from the synchronized attractor as a function of their distance from the corresponding invariant manifold. The second scaling law is related to the concept of uncertain initial conditions. An initial condition is always determined up to a given uncertainty, which can be represented in the phase space by a multidimensional sphere centered at the initial condition, whose radius is equal to the maximum uncertainty. An initial condition is deemed uncertain if the basin boundary intercepts this sphere. Therefore, the second scaling law results from computing the fraction of uncertain initial conditions as a function of the uncertainty radius near the attractor with a riddled basin.

We verified numerically that both scaling relations are power laws and determined their corresponding scaling exponents. Furthermore, we compared the exponents of the power laws with the predictions obtained from the OAKSY stochastic model, which utilizes the probability distribution function for the maximal finite-time transversal Lyapunov exponents. We showed that within the range of validity of the stochastic model, particularly near the so-called blowout bifurcations, it accurately predicts the scaling exponents even in high-dimensional coupled systems.

Another issue we have studied is the severe breakdown of shadowability of chaotic trajectories due to unstable dimension variability. The latter is characterized by a lack of shadowability due to the nonexistence of a continuous decomposition of the tangent space into stable and unstable manifolds. An important practical consequence of unstable dimension variability is that computer-generated (pseudo)-trajectories, which are always corrupted by truncation and one-step errors, may not be shadowed by true chaotic trajectories of the dynamical system. For systems possessing an invariant subspace, such as those with a synchronized chaotic attractor, a fingerprint of unstable dimension variability is the existence of positive and negative finite-time transversal Lyapunov exponents.

The maximum intensity of unstable dimension variability occurs when there are as many positive as negative finite-time exponents, in other words, when a blowout bifurcation occurs. In this case, the stochastic OAKSY model appears to produce an appropriate description of the dynamics in the directions transversal to the invariant chaotic attractor. Moreover, after a blowout bifurcation occurs, the latter becomes transversely unstable, and while it is still a chaotic invariant set, it is no longer attracting on average. We observed that, in our coupled system, unstable dimension variability occurs for most values of the tunable parameter, a situation that seems to be quite common in high-dimensional dynamical systems of physical interest. Hence, although our conclusions were drawn from a specific model, the behavior and properties we described

15 September 2024 03:59:26

Published under an exclusive license by AIP Publishing

are expected to be present in a wider class of dynamical systems possessing a chaotic attractor lying on an invariant subspace.

DEDICATION

This work was dedicated to the memory of Professor Jason A. C. Gallas.

ACKNOWLEDGMENTS

This study was financed in part by the "Coordenação de Aperfeiçoamento de Pessoal de Nível Superior"—Brazil (CAPES)—Finance Code 001 and by the "Conselho Nacional de Desenvolvimento Científico e Tecnológico"—Brazil (CNPq) under Grant Nos. 403120/2021-7 and 301019/2019-3.

AUTHOR DECLARATIONS

Conflict of Interest

The authors have no conflicts to disclose.

Author Contributions

Bruno M. Czajkowski: Conceptualization (equal); Data curation (equal); Formal analysis (equal); Investigation (equal); Methodology (equal); Software (equal); Validation (equal); Visualization (equal); Writing – original draft (equal); Writing – review & editing (equal). **Ricardo L. Viana:** Conceptualization (equal); Formal analysis (equal); Methodology (equal); Project administration (equal); Supervision (equal); Visualization (equal); Writing – original draft (equal); Writing – review & editing (equal).

DATA AVAILABILITY

The data that support the findings of this study are available from the corresponding author upon reasonable request.

APPENDIX: NUMERICAL METHOD FOR OBTAINING UNSTABLE PERIODIC ORBITS

We obtained some unstable periodic orbits embedded in the chaotic attractor of our coupled system (see Table I), in order to verify the conditions of riddling as well as the existence of unstable dimension variability. These periodic orbits were obtained by the Newton–Raphson–Mees method, described in Ref. 24. In this Appendix, we briefly describe how this method works.

Given a vector field

$$\frac{dx}{dt} = F(x), \tag{A1}$$

where $x \in \mathbb{R}^n$, we denote by $\phi(x_0, t)$ the solution $x(t)$ of this system for an initial condition $x_0 = x(0)$. We also define

$$G(x_0, t) = \phi(x_0, t) - x_0. \tag{A2}$$

A periodic orbit of period T can be obtained by the zeroes of $G(x_0, T)$. We consider the variation of G,

$$\Delta G(x_0, T, \Delta x_0, \Delta T) = \left(\frac{d\phi(x_0, T)}{dx_0} - I \right) \Delta x_0 + F(\phi(x_0, T))\Delta T, \tag{A3}$$

where I is the identity matrix of order n.

The Newton–Raphson–Mees method consists of iterating a map (x_i, T_i) and at each step finding for what changes $(\Delta x_i, \Delta T_i)$, the condition

$$G(x_i, T_i) + \Delta G(x_i, T_i, \Delta x_i, \Delta T_i) = 0 \tag{A4}$$

is satisfied. If this map converges to (x_0, T), then $G(x_0, T) = 0$, and the condition for periodicity of the orbit is fulfilled. However, the system described by Eq. (A4) is a $n \times n$ linear system with $n + 1$ variables (n for x_0 and 1 for T) so that we have to impose a constraint. This can be done by restricting the changes in the position to be orthogonal with respect of the flux, that is,

$$F(\phi(x_i, T_i)) \cdot \Delta x_i = 0. \tag{A5}$$

Given an initial guess for the period T_0 and for a point x_0, we construct a map of the form

$$(x_{i+1}, T_{i+i}) = (x_i, T_i) + 2^{-m}(\Delta x_i, \Delta T_i), \tag{A6}$$

where $m \in \mathbb{N}$ is a damping coefficient introduced so as to increase the convergence of the Newton–Raphson method. The vector $(\Delta x_i, \Delta T_i)$ is calculated by solving the linear system

$$\Delta G(x_i, T_i, \Delta x_i, \Delta T_i) = -G(x_i, T_i), \tag{A7}$$

supplied with the constraint given by Eq. (A5).

When iterating the map, we consider two types of errors. The first is related to how close $\phi(x_i, T_i)$ is of x_i, given by $e_i^g = |G(x_i, T_i)|$. The other is associated with the rate of convergence of the method, given by $e_i^m = |(\Delta x_i, \Delta T_i)|$, where $|\cdots|$ stands for the Euclidean norm in $\mathbb{R}^n$. We assumed that the map converged to a periodic point if both e_i^g and e_i^m are less than 10^{-7}. The initial guesses for the position x_0 are points in the chaotic attractor, randomly chosen according to its natural measure, while the initial periods T_0 are uniformly chosen in the interval $[0, 100]$.

REFERENCES

[1] J. Alexander, J. A. Yorke, Z. You, and I. Kan, Int. J. Bifurc. Chaos Appl. Sci. Eng. **02**, 795–813 (1992).
[2] S. W. McDonald, C. Grebogi, E. Ott, and J. A. Yorke, Phys. D: Nonlinear Phenom. **17**, 125–153 (1985).
[3] J. Aguirre, R. L. Viana, and M. A. F. Sanjuán, Rev. Mod. Phys. **81**, 333–386 (2009).
[4] L. M. Pecora and T. L. Carroll, Phys. Rev. Lett. **64**, 821–824 (1990).
[5] E. Ott, J. C. Sommerer, J. C. Alexander, I. Kan, and J. A. Yorke, Phys. Rev. Lett. **71**, 4134–4137 (1993).
[6] L. M. Pecora, T. L. Carroll, G. A. Johnson, D. J. Mar, and J. F. Heagy, Chaos **7**, 520–543 (1997).
[7] E. Ott and J. C. Sommerer, Phys. Lett. A **188**, 39–47 (1994).
[8] P. Ashwin, J. Buescu, and I. Stewart, Phys. Lett. A **193**, 126–139 (1994).
[9] R. L. Viana, C. Grebogi, S. E. D. S. Pinto, S. R. Lopes, A. M. Batista, and J. Kurths, Phys. Rev. E **68**, 067204 (2003).
[10] J. F. Heagy, T. L. Carroll, and L. M. Pecora, Phys. Rev. Lett. **73**, 3528–3531 (1994).
[11] E. Ott, J. Alexander, I. Kan, J. Sommerer, and J. Yorke, Phys. D: Nonlinear Phenom. **76**, 384 (1994).
[12] A. Elwakil, S. Ozoguz, and M. Kennedy, IEEE Trans. Circuits Syst. I Regul. Pap. **49**, 527 (2002).
[13] S. Camargo, R. L. Viana, and C. Anteneodo, Phys. Rev. E **85**, 036207 (2012).
[14] E. N. Lorenz, J. Atmos. Sci. **20**, 130–141 (1963).

15 September 2024 03:59:26

Published under an exclusive license by AIP Publishing

[15]A. Elwakil, S. Ozoguz, and M. Kennedy, Int. J. Bifurc. Chaos Appl. Sci. Eng. **13**, 3093 (2003).
[16]L. Chua, M. Komuro, and T. Matsumoto, IEEE Trans. Circuits Syst. **33**, 1072–1118 (1986).
[17]S. Ozoguz, A. Elwakil, and M. Kennedy, Int. J. Bifurc. Chaos Appl. Sci. Eng. **12**, 1627 (2002).
[18]G. Benettin, L. Galgani, A. Giorgilli, and J.-M. Strelcyn, Meccanica **15**, 9–20 (1980).
[19]G. Benettin, L. Galgani, and J.-M. Strelcyn, Phys. Rev. A **14**, 2338–2345 (1976).
[20]R. F. Pereira, S. Camargo, S. E. de S. Pinto, S. R. Lopes, and R. L. Viana, Phys. Rev. E **78**, 056214 (2008).
[21]J. C. Sommerer and E. Ott, Nature **365**, 138–140 (1993).
[22]Y.-C. Lai, C. Grebogi, J. A. Yorke, and S. C. Venkataramani, Phys. Rev. Lett. **77**, 55–58 (1996).
[23]R. L. Viana, S. E. de S. Pinto, J. R. R. Barbosa, and C. Grebogi, Int. J. Bifurc. Chaos Appl. Sci. Eng. **13**, 3235–3253 (2003).
[24]Y. Saiki, Nonlinear Process. Geophys. **14**, 615 (2007).
[25]C. Sparrow, *The Lorenz Equations: Bifurcations, Chaos, and Strange Attractors* (Springer, New York, 1982).
[26]D. Viswanath, Nonlinearity **16**, 1035–1056 (2003).
[27]C. Grebogi, S. W. McDonald, E. Ott, and J. A. Yorke, Phys. Lett. A **110**, 1 (1985).
[28]C. Grebogi, S. W. McDonald, E. Ott, and J. A. Yorke, Phys. Lett. A **99**, 415–418 (1983).
[29]C. Grebogi, E. Kostelich, E. Ott, and J. A. Yorke, Phys. D: Nonlinear Phenom. **25**, 347–360 (1987).
[30]J. C. Vallejo and M. A. F. Sanjuan, *Predictability of Chaotic Dynamics: A Finite-Time Lyapunov Exponents Approach* (Springer International Publishing, 2019).
[31]E. Kostelich, I. Kan, C. Grebogi, E. Ott, and J. Yorke, Phys. D: Nonlinear Phenom. **109**, 81 (1997).
[32]J. Guckenheimer and P. Holmes, *Nonlinear Oscillations, Dynamical Systems, and Bifurcations of Vector Fields*, Applied Mathematical Sciences (Springer, New York, 2013).
[33]C. Grebogi, L. Poon, T. Sauer, J. A. Yorke, and D. Auerbach, "Shadowability of chaotic dynamical systems," in *Handbook of Dynamical Systems* (Elsevier, 2002), pp. 313–344.
[34]R. Bowen, J. Differ. Equ. **18**, 333–339 (1975).
[35]J. A. C. Gallas, in *Recent Trends in Chaotic, Nonlinear and Complex Dynamics*, edited by J. Awrejcewicz, R. Shanmuganathan, and M. Ragulskis (World Scientific, 2021), pp. 275–298.
[36]C. Grebogi, E. Ott, and J. A. Yorke, Phys. Rev. Lett. **57**, 1284–1287 (1986).
[37]T. Sauer, C. Grebogi, and J. A. Yorke, Phys. Rev. Lett. **79**, 59–62 (1997).
[38]R. Abraham and S. Smale, in *Proceedings of Symposia in Pure Mathematics* (AMS, 1970), Vol. 14, p. 5.
[39]F. J. Romeiras, C. Grebogi, E. Ott, and W. Dayawansa, Phys. D: Nonlinear Phenom. **58**, 165–192 (1992).
[40]G. T. Kubo, R. L. Viana, S. R. Lopes, and C. Grebogi, Phys. Lett. A **372**, 5569–5574 (2008).
[41]Y. Saiki, M. A. F. Sanjuán, and J. A. Yorke, Chaos **28**, 103110 (2018).
[42]E. Barreto and P. So, Phys. Rev. Lett. **85**, 2490–2493 (2000).
[43]Y.-C. Lai, D. Lerner, K. Williams, and C. Grebogi, Phys. Rev. E **60**, 5445–5454 (1999).
[44]R. L. Viana and C. Grebogi, Phys. Rev. E **62**, 462–468 (2000).
[45]R. L. Viana, S. E. D. S. Pinto, and C. Grebogi, Phys. Rev. E **66**, 046213 (2002).
[46]S. Dawson, C. Grebogi, T. Sauer, and J. A. Yorke, Phys. Rev. Lett. **73**, 1927–1930 (1994).

15 September 2024 03:59:26

Published under an exclusive license by AIP Publishing